Upward mass transport and alloying during the growth of Co on Cu(111)

Quang Huy Vu and Karina Morgenstern
Physical Chemistry I, Ruhr-Universität Bochum, Universitätsstrasse 150, D-44801 Bochum, Germany
(Received 19 July 2016; revised manuscript received 21 December 2016; published 17 March 2017)

Co growth on Cu(111) was investigated at several temperatures between 120 K and 300 K by variable-temperature fast-scanning tunneling microscopy at submonolayer coverage. Islands nucleate heterogeneously at step edges and homogeneously on terraces. The height and area distribution difference between these two types of differently nucleated islands is attributed to a step edge alloy. Furthermore, the transformation from one-monolayer high islands to two-monolayer high islands is followed in time-lapsed sequences between 145 and 165 K. A surprising low-energy barrier for upward mass transport of $E_{\mathrm{upward}} \approx (0.15 \pm 0.04)$ eV is determined for islands on terraces. At 120 and 150 K, the terrace islands are pure Cu; in contrast, at room temperature, terrace islands larger than $\approx$120 nm^2 alloy at their border.

DOI: 10.1103/PhysRevB.95.125423

I. INTRODUCTION

Thin-film technology plays a crucial role in science and technology. Studies in both theory and experiment have revealed many astonishing physical and chemical properties of thin films on metal surfaces [1,2]. In particular, the study of ferromagnetic films is attracting widespread interest in different fields, such as magnetic data storage and spin electronic devices [3,4]. Indeed, "spin electronics" has been extensively studied since the 1960s, especially the conductive properties of the ferromagnetic metals Fe, Ni, Co and their alloys [5–7]. Moreover, it is well known that the properties of thin-film growth strongly depend on how the guest atoms arrange on the host metal surface [8,9].

In this study, we focus on the submonolayer growth of the heteroepitaxial system Co on Cu(111). Previous studies of this system gave promising results in structure [10–14], electronic properties [15–20], and magnetic properties [21,22]. The small lattice mismatch of $\approx$1.9% between Co and Cu is expected to lead to similar structures as in homoepitaxial growth. However, a possible formation of intermixed islands at room temperature was discussed briefly [23]. So far, growth was investigated at room temperature, where islands with bilayer height grow on terraces [24,25] following the fcc stacking of the Cu substrate [26,27]. Though the decoration of step edges by Co islands was observed, this heterogeneous nucleation was not discussed [24,25].

According to calculations [12], Co atoms can ascend to the second layer through the exchange mechanism at the step edges of monatomic layer islands with energy barriers of 0.66 and 0.91 eV for an *A* and a *B* step, respectively. This process has not yet been observed directly.

Previous studies for growth below room temperature suggest that Co atoms aggregate on Cu(111) to ramified islands on terraces due to limited diffusion along the step edges of the islands [12].

In this paper, we investigate the growth of Co on Cu(111) in the submonolayer regime of 0.03 to 0.04 ML at low temperature (120 and 150 K) and compare it to room-temperature growth. We discuss island shapes and densities of both islands nucleated on terraces and at step edges at the three investigated temperatures, and reveal the difference between the two nucleation regions. Moreover, fast-scanning scanning tunneling microscopy (STM) is used to follow the upward mass transport of Co atoms from the first to the second layer between 145 and 165 K in real time. The activation energy for this transition process is surprisingly low, which is explained by the ramified shape of the islands.

II. EXPERIMENT

The experiments were performed in a standard ultrahigh vacuum (UHV) chamber (base pressure $\leqslant 4 \times 10^{-10}$ mbar) consisting of a measurement chamber, which contains the usual equipment for sputtering, annealing and the STM, and a separate deposition chamber. Transfer between the preparation stages and the STM is done by means of a transfer rod without breaking the vacuum. The commercial variable-temperature fast-scanning STM (SPECS "STM 150 Aarhus") can operate with fast-scanning speed (3–4 images/min) within the temperature range from 90 to 350 K and with a scan range of 1500 $\times$ 1500 nm. The STM consists of a single tube scanner for three-dimensional motion during scanning and an inchworm motor for coarse approach. The STM enables repeated recording of images at the same spot of the sample (called movies).

The Cu(111) surface was cleaned by repeated cycles of sputtering with Ar^+ (1.3 keV, $I \approx 12$ μA for 15 min) and annealing up to 900 K for 40 min. Submonolayer amounts of Co were evaporated by a home-built molecular beam evaporator (MBE) onto the sample held by a transfer rod. The evaporation material with a purity of 99.99% was outgassed under UHV conditions until the pressure stayed in a range of 10^{-10} mbar during evaporation. A constant evaporation rate is established by means of a quartz crystal microbalance (QCM). The deposition rate on the QCM is determined to be (3.0 ± 0.6) ML/min, in which one monolayer (ML) is defined as one adsorbate atom per surface atom. Because the distance from the evaporator to the sample is approximately 45 cm, coverages are much more precisely determined from STM images than from the QCM close to the evaporator. Co coverages between 0.03 and 0.04 ML were obtained for all measurements, suggesting a deposition rate of $(3.5 \pm 0.5) \times 10^{-2}$ ML/min.

Co was deposited at (117 ± 2) K, (144 ± 3) K, and at room temperature. The sample was transferred within minutes

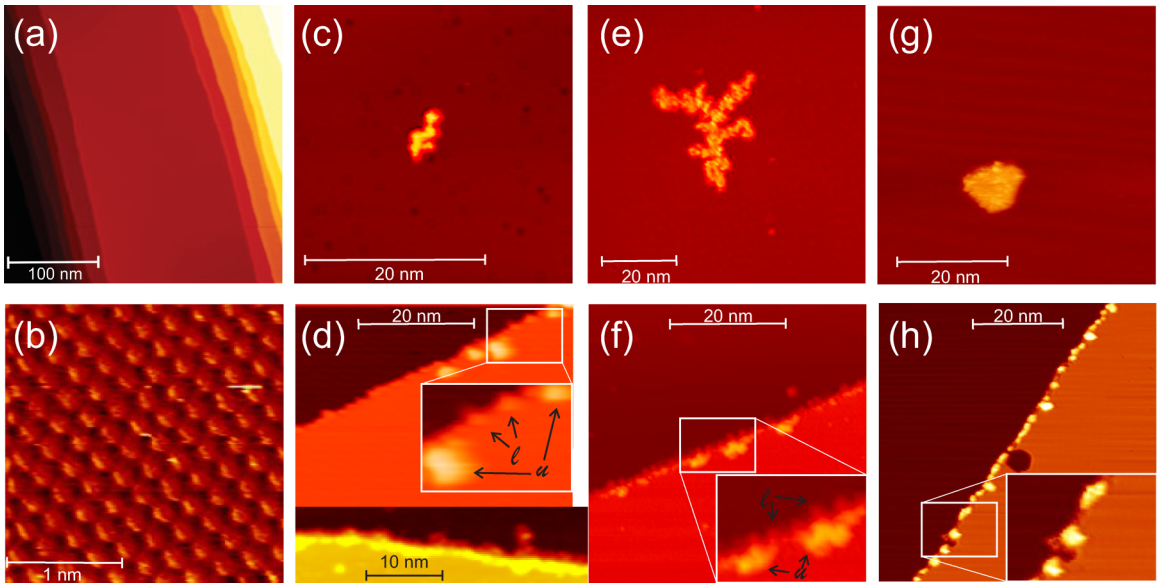

FIG. 1. Cu(111) surface before and after Co deposition. (a),(b) STM images of pristine surface before deposition: (a) large-scale image, (b) atomic resolution. (c)–(h) 0.04 ML Co on terraces and at step edges deposited at (c),(d) 120 K. Lower inset: step edge at higher coverage to make nucleation at lower step edge visible; at (e),(f) 150 K and (g),(h) room temperature (RT). Insets: magnification by a factor of 2. Nucleation at lower and at upper step edge is marked. Tunneling parameters: (a) $V_t = -805$ mV, $I_t = 0.5$ nA, RT; (b) -175 mV, 1.4 nA, RT; (c),(d) -860 mV, 0.5 nA, 120 K; Inset: -884 mV, 0.53 nA; (e),(f) 1160 mV, 0.07 nA, 150 K; (g),(h) -860 mV, 0.33 nA, RT.

to the STM after deposition. Within the STM, the sample temperature increases at a rate of 10 K/h.

The prepared structures were investigated at around 120 K, between 145 and 165 K, and at room temperature.

All the characteristic Co island values, such as height, area, and coverage, were determined by SPIP (Image Metrology) and WSXM [28] softwares. The area of the islands is determined by the island region that is higher than its half maximum height (FWHM). The values given are upper limits of the real area due to tip convolution effects. The heights given correspond to the highest points of the islands. A bilayer high island thus denotes an island which is partly higher than a monolayer one.

III. RESULTS

A. Shape of Co islands on Cu (111) at different temperatures

Before discussing the growth mode at different temperatures in detail, we compare the growth structures qualitatively at the same coverage (Fig. 1). After the cleaning procedure, the surface exhibits large terraces separated by bundles of smaller terraces [Fig. 1(a)]; here the width of the largest terrace is around 170 nm. The step density of the used sample is approximately 1 step/20 nm. The orientation of the close-packed rows is determined from images with atomic resolution [Fig. 1(b)]. At all temperatures, well-separated islands are formed on the terraces [Figs. 1(c), 1(e), 1(g)] and grown at step edges [Figs. 1(d), 1(f), 1(h)]. The Co islands on the terraces are ramified at 120 and 150 K [Figs. 1(c) and 1(e)]. At 150 K, the islands grow with three prominent branches separated by around 120°, and some additional small branches attached to the thick branches [Fig. 1(e)]. The distinct angles are indicative of a growth mode that is influenced by the directionality of the surface [29–32]. At 300 K, the islands are compact [Fig. 1(d)].

In contrast to the growth on the terraces, the Co islands at step edges are compact at all temperatures [Figs. 1(d), 1(f), 1(h)]. At 120 and 150 K, Co islands grow at the upper and lower edges of the step, while at 300 K, growth of Co islands is only at the upper edge. The decoration of the steps by Co islands [Fig. 4(a)] is also found in heteroepitaxial growth on Cu(111), such as Fe/Cu(111) and Co/Cu(111), at room temperature [24,25,33]. Note that at room temperature, we observe hexagonal vacancy islands close to the step edge [Fig. 1(h)]. Quantitative properties of the Co islands nucleated both homogeneously on terraces and heterogeneously at step edges will be discussed in the next sections separately for each temperature for a coverage of 0.03 to 0.04 ML.

B. Growth of Co on Cu(111) at 120 K

At 120 K, Co islands nucleate exclusively at the step edges of terraces with a mean terrace width of (25.0 ± 2.7) nm [Fig. 2(a)], while on larger terraces they also nucleate on terraces, e.g., for a width of (121.0 ± 0.5) nm [Fig. 2(b)]. Indeed, the island density ρ depends on the terrace width W with a sharp transition between 27 and 44 nm [Fig. 2(c)]. On a crystal with high step density as used here (approximately 1 step/20 nm), the majority of the Co islands are grown at step edges at 120 K. Thus, Co atoms are able to diffuse to the step edges at the deposition temperature of 120 K and then either stick to them with high probability or form nuclei close to them [1]. For systems without an additional step edge barrier, sticking to the step edge is expected for atoms approaching the step edge from both directions because of the larger coordination number at the lower step edge [31]. However, for surfaces with an additional step edge barrier, as Cu(111), sticking is expected only to the lower step edge. The large nucleation density on the upper terrace observed

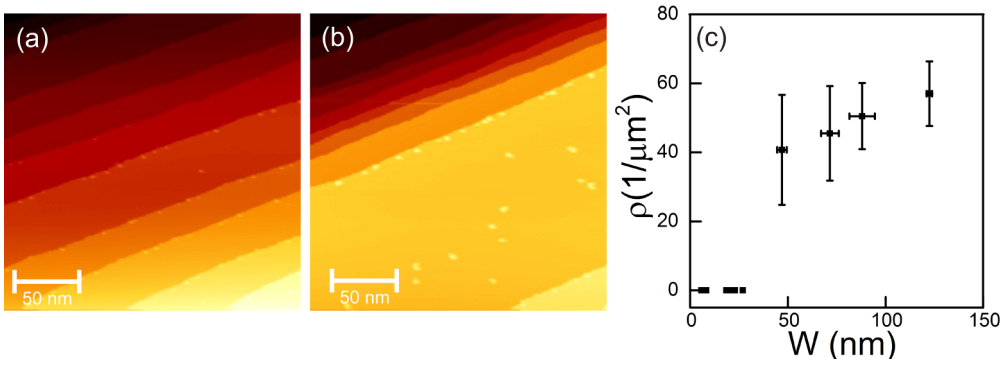

FIG. 2. Growth of Co islands at 120 K (−805 mV, 0.6 nA, 0.03 ML, 120 K): (a) region of surface with small terrace widths, $\langle d \rangle = (25 \pm 2.7)$ nm; (b) region with one large terrace of (121 ± 0.5) nm; and (c) relation between island density ρ and terrace width W.

here demands an additional explanation. In combination with a denuded zone close to the step edge, it indicates that the Co atoms are trapped close to the step edges, i.e., that their diffusion barrier is increased substantially.

Indeed, according to empiric interatomic potential calculations [23], Co atoms attach to the step edges through two pathways, at the very early stages of growth (Fig. 3). In the first pathway, Co atoms from the upper terrace push one Cu atom perpendicularly out of the step edge and replace it through an exchange process [path E, Fig. 3(a)]. In the second pathway, the Co atoms from the lower terrace attach to the atomic rows parallel to the edge through a diffusion process [path D, Fig. 3(a)]. These dynamic processes alter the diffusion barriers, as shown in Fig. 3(b). The diffusion energies of a Co atom from the Co atoms labeled "1" and "2" to the Cu terrace increase by 0.24 and 0.10 eV, respectively, as compared to an atom diffusing on the pristine Cu surface with a diffusion energy of 0.04 eV [12,23]. As a result, these positions are nucleation centers on the upper side of the step edge for subsequently arriving Co atoms. While further attachment of Co at the lower step edge will passivate the step towards the exchange processes [Fig. 1(f)], this will not affect the growth of the islands on the upper step edge in their growth phase.

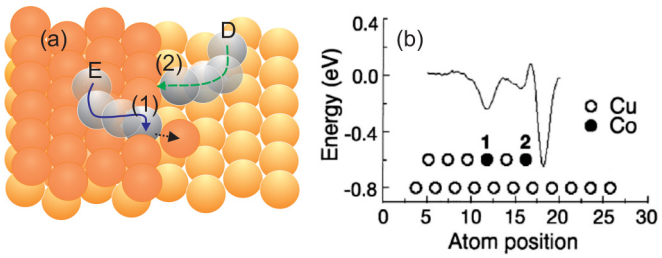

FIG. 3. Origin of an additional energy barrier at step edges, adapted from Ref. [23] (with permission of author), illustrating a (a) sketch of mobile Co atoms reaching the step edge based on Monte Carlo calculations [23]. The darker orange balls are Cu atoms on the upper terrace, while the lighter orange balls are on the lower terrace. The gray balls are Co atoms. The solid and dashed arrows indicate the trajectory of the mobile Co atoms through the exchange process (E) and diffusion process (D), respectively. (b) Energy profile from static relaxations [23] for the diffusion of a Co atom after the incorporation of other Co atoms at step edges.

After clarifying the nucleation of Co islands on the upper step edge, we now characterize these islands geometrically. The height of Co islands on the step edges is obtained from line profiles as shown in Fig. 4(b) along the line indicated in Fig. 4(a). The dashed line marks the measured height of the Co island, revealing a height of ≈0.2 nm with respect to the upper terrace. Based on the first maximum in the height distribution from measuring the height of several islands [see Fig. 4(c)], we determine an average value of (0.20 ± 0.02) nm for the Co islands grown at step edges at 120 K. This height is identical to the height of (0.20 ± 0.01) nm measured at room temperature for monatomic layer high Co islands on Cu(111) surface [24,25]. In addition, we note that the height of Co islands is consistent with the height of 0.209 nm for Cu steps [Fig. 4(b)]. The majority of the islands is thus of monolayer height. There are very few islands with a height of $(0.38 \pm$

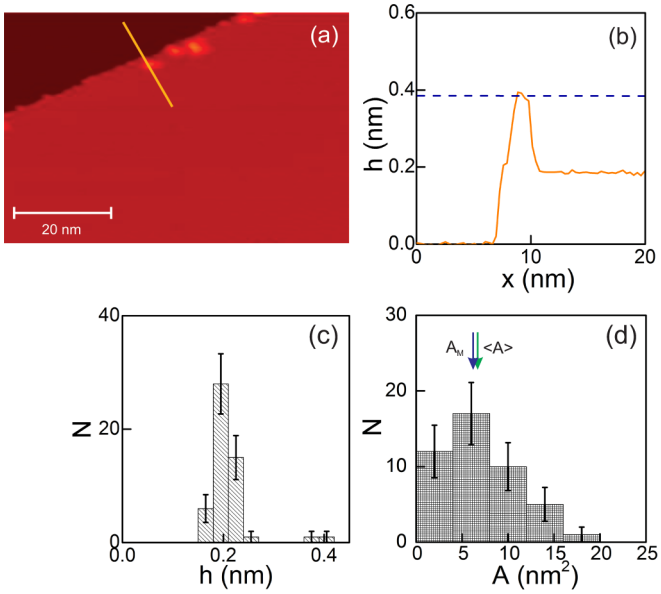

FIG. 4. Co island growth at step edges at 120 K: (a) STM image of 0.03 ML (−805 mV, 0.4 nA, 120 K); (b) Line profile along the line across the step edge, as shown in (a). The dashed line marks the measured height of the Co island at the upper edge of the step. (c) Height distribution. (d) Area distribution. A_M: median value. $\langle A \rangle$: mean value.

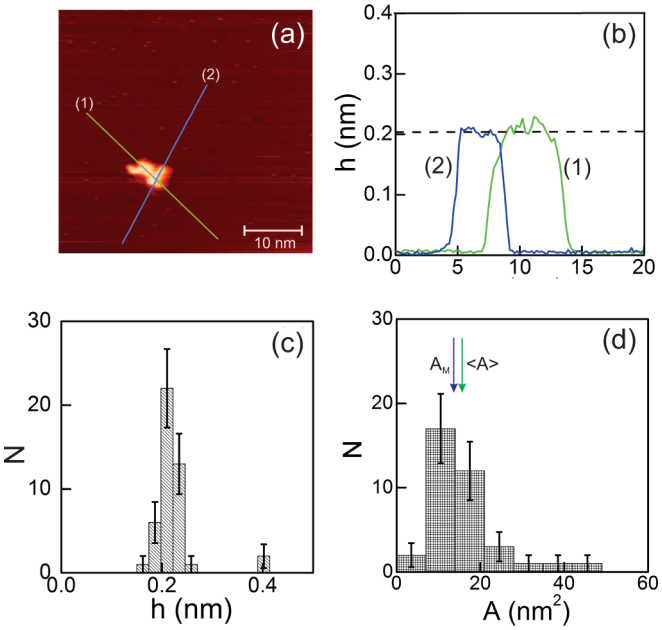

FIG. 5. Growth of Co islands on terraces at 120 K: (a) STM image ($V_t = -800$ mV, $I_t = 0.5$ nA, 0.03 ML, 120 K); (b) Line profiles along the lines shown in (a). The dashed line indicates the measured height of the Co island. (c) Height distribution. (d) Area distribution. $\langle A \rangle$: mean value. A_M: median.

0.02) nm (percentage about 4%). This low percentage suggests that these higher islands result from statistical deposition of some atoms on top of existing islands. We conclude that no upward mass transport takes place at 120 K.

The area of the islands varies from 1 to 20 nm^2 [Fig. 4(d)] with a mean island area $\langle A \rangle$ of (7.2 ± 3.9) nm^2 and a median A_M of 6.9 nm^2 [Fig. 4(d)]. The area distribution shows the typical behavior as described in the theory of nucleation and growth by Venables with one maximum and two asymmetric flanks [1,31,34].

We summarize that during growth at 120 K, the step edge is modified such that Co atoms are trapped close to the upper step edge. In this well, islands nucleate according to classical nucleation theory as islands of monolayer height.

At the same temperature of 120 K, the island shape is ramified on terraces, in contrast to the compact island shape at the step edges. For the example in Fig. 5(a), there are two main branches and one minor one. The angle between the branches is approximately 120°. The average width of the branches is (1.38 ± 0.04) nm. The shape and fractal dimension of these islands will be discussed in more detail elsewhere [35].

With the same procedure as above, we identify islands of two different heights, (0.21 ± 0.02) and (0.40 ± 0.01) nm [Figs. 5(b) and 5(c)]. Also on the terraces, the percentage of islands with second layer nucleation is very small, only about 5%, consistent with a statistical deposition of Co in the second layer.

The island area varies in a wider range, from 1 to 50 nm^2, than the islands on the step edges. The mean size of $\langle A \rangle = (15.9 \pm 8.4)$ nm^2 is around twice the one at the step edges [Fig. 5(d)]. Nonetheless, the size distribution also follows the shape predicted by the theory of Venables [1,31,34], for which the mean approximately equals the median at around $A_M = 13.8$ nm^2.

In conclusion, all parameters, size range, mean, and median are about twice as large for islands on the terraces as on the step edges. This is consistent with the reduced diffusivity of the Co atoms close to step edges compared to the one on terraces. Most importantly, the growth on both terraces and step edges shows a predominance of monatomic high islands, which means that upward mass transport does not occur at 120 K.

C. Growth of Co on Cu(111) at 145 K to 165 K

It is surprising that Co islands grown at 120 K are predominately monatomic layer high, while bilayer high islands were reported at room temperature [24,25]. This suggests that bilayer islands are thermodynamically preferred, but material transport from the border of an island to its top is kinetically limited.

In order to find the temperature at which the kinetic limitation of upward mass transport is surmountable, we followed the transformation from monolayer high islands to islands with atoms appearing in the second layer between 145 and 165 K for islands initially deposited at 144 K. At 165 K, an upward mass transport takes place on the time scale of a few minutes (Fig. 6). At four different temperatures (146, 149, 160, and 165 K), we observed transport to the second layer within tens of seconds between subsequent images.

In order to determine the energy barrier for the upward mass transport from these experimental observations, we use the theory of diffusion-limited ripening [36]. In this theory, the mass transport of atoms from or to an island is considered. In the original geometry, atoms from an island detach and then diffuse over the terrace to a surrounding sink [37]. This geometry has been adapted to a situation where the atom flow is reversed and atoms coming from the surroundings fill a vacancy island in the middle [38]. The change in island size is induced by gradients in the chemical potential (the adatom density). The theory allows one to determine the detachment barrier from the island border and the diffusion energy over the terrace in the first case. Here, we adapt the theory to determine the energy barrier for the upward mass transport to the existing island. Application of this theory is necessary because the number of atoms available for ascending to the island depends on the island size.

Adaption of the most general formula [36,39,40] to our case, where the rate limiting case is at the border of the original island, yields

$$\frac{dA}{dt} \approx -\nu \exp\left[-\frac{E_d + E_{\text{upward}}}{k_B T}\right], \tag{1}$$

where ν is a temperature independent prefactor and $E_d + E_{\text{form}} = E_A$ corresponds to the activation energy for the upward mass process, with E_d the diffusion energy on a terrace far away from step edges and E_{upward} the additional barrier for upward mass transport.

In order to determine the energy barrier, we plot the change in area of the monatomic layer island, half logarithmically, versus the inverse temperature. The points in the Arrhenius plot fall in a straight line, yielding an activation energy of

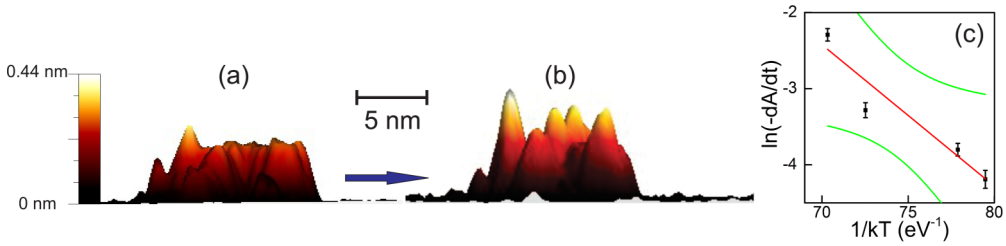

FIG. 6. Transport of atoms from the first to the second layer of an island on the terrace: (a) Three-dimensional (3D) STM image on false-color scale of an island; (b) 3D STM image of the same island after 2 min ($U_t = -860$ mV, $I_t = 0.6$ nA, 0.04 ML, 165 K); (c) Arrhenius plot: the red line is an apparent linear fit yielding $E_A \approx (0.19 \pm 0.04)$ eV and a prefactor $\nu \approx (1.8 \pm 0.5) \times 10^{11}/\mathrm{s}$. Green curved lines show the confident band of the fitting process.

$E_A = (0.19 \pm 0.04)$ eV [Fig. 6(c)]. Based on the theory discussed above, the activation energy consists of the energy E_{upward} for Co atoms moving upward from the first to the second layer of the island and the energy barrier E_d for atoms diffusing to this monolayer island. The terrace diffusion energy on of Co on Cu(111) was determined to be 0.04 eV [12,25]. This yields $E_{\mathrm{upward}} = (0.15 \pm 0.04)$ eV.

Surprisingly, the activation barrier determined by STM measurements is considerably lower than the theoretical results. Activation energies for upward motion of an atom via the exchange process were determined to be 0.66 eV at a B step and 0.91 eV at an A step [12]. Note that theoretical results are calculated for processes at straight step edges of an equilibrium-shaped island, while experimental results are achieved by examining ramified islands. This suggests that different barriers result from a difference in step morphology. This assumption is supported by the results of the growth of Pt on Pt(111), which showed that kink positions have a lower activation barrier than step positions [41,42]. Therefore, we conclude that the upward mass transport at low temperature for islands of irregular shape mainly proceeds at kink positions with a much lower energy barrier than the process at straight step edges, which allows the upward mass transport at cryogenic temperature. Note that the number of kinks on the more compact islands at the step edges is also considerable because of their small size.

Finally, we critically discuss whether we have determined the ascending barrier for Co atoms or for Cu atoms. If it was Cu atoms ascending, then Cu must have been involved in the island formation at 150 K. This is unlikely because the extended investigation of the kinetics of Cu islands on Cu(111) and step edge fluctuations on the same surface showed that the gas of Cu atoms on Cu(111) at the deposition temperature of 150 K is negligible [43]. Another source of Cu adatoms could be those released from the surface due to Co exchange. However, our extended studies showed that there is no exchange process possible on terraces at this temperature, in agreement with theoretical predictions. Finally, previous studies showed that bilayer high Co islands form on Cu(111) [24,25], in agreement with the bilayer preference calculated by theory. This leads us to the conclusion that the island consists entirely of Co at low temperature and thus it must be the Co that moves to the second layer.

As discussed above, the upward mass transport is observed on the time scale of the experiment between 145 K to 165 K. We thus expect that at around this temperature, more islands should exhibit atoms in the second layer than at a random deposition of Co atoms on top of existing islands. Hence, we investigated the growth at around 150 K in detail, both at step edges and on terraces.

The distribution of Co islands on step edges and terraces is very similar for the growth at 150 K as compared to the growth at 120 K (Fig. 7). No Co islands grow on terraces with a mean width of (20.1 ± 7.2) nm [Fig. 7(a)], but a high density of islands grows on a terrace with a width of (244 ± 2) nm [Fig. 7(b)]. The transition is between 23 and 45 nm [Fig. 7(c)]. Again, for the small average terrace width of our sample, this implies that the majority of islands grow at the step edges.

However, the Co island growth at step edges at 150 K differs quantitatively from the growth mode of islands at 120 K with

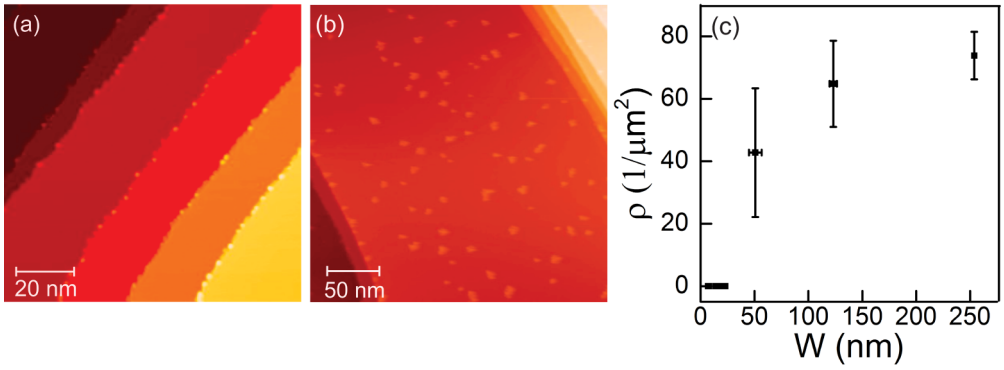

FIG. 7. Growth of Co islands at ≈150 K: (a) region of surface with small terraces, $\langle d \rangle = (20.1 \pm 7.2)$ nm (860 mV, 0.5 nA, 146 K, 0.03 ML); (b) region of surface with a wide terrace, $d = (244 \pm 2)$ nm (−800 mV, 0.42 nA, 154 K, 0.04 ML); and (c) dependence of island density ρ on terrace width W.

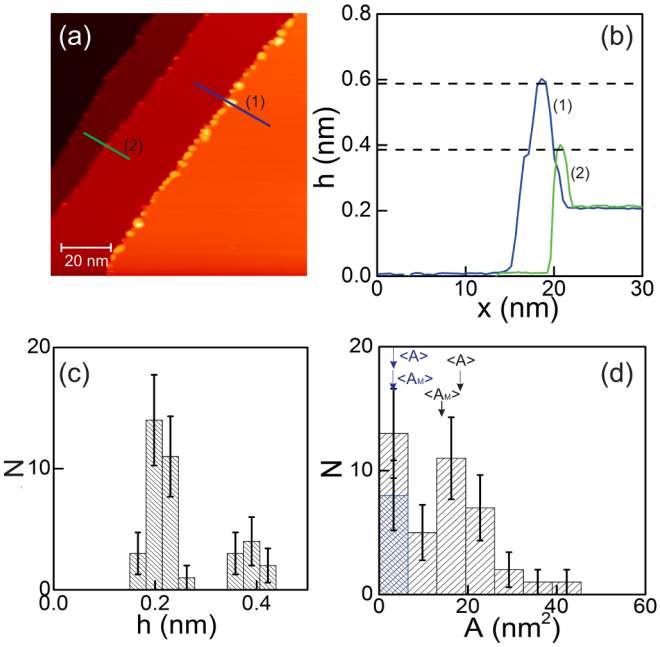

FIG. 8. Co island growth at step edges at ≈150 K: (a) STM image with a mean terrace width of (20.1 ± 7.2) nm (860 mV, 0.5 nA, 146 K, 0.03 ML); (b) Line profile across step edges along the lines as shown in (a). Dashed lines mark measured heights of the Co islands. (c) Height distribution. (d) Area distribution of all islands in gray. Bilayer high island distribution in blue. A_M is median value. $\langle A \rangle$ is mean value.

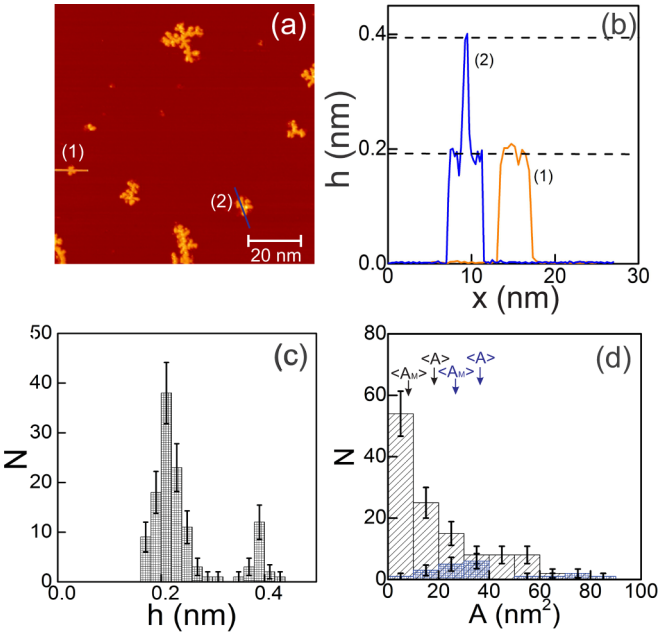

FIG. 9. Growth of Co islands on terraces at ≈150 K: (a) STM image of the Co islands (−1740 mV, 0.1 nA, 150 K, 0.04 ML); (b) Line profiles along the lines as shown in (a). Dashed lines mark the measured height of Co islands. (c) Height distribution. (d) Area distribution of all islands in gray; only bilayer high island in blue. A_M is the median value. $\langle A \rangle$ is the mean value.

respect to their height and area [Fig. 8(a)]. The percentage of islands with atoms in the second layer with (0.39 ± 0.02) nm height [Figs. 8(b) and 8(c)] is, at 26%, around five times larger than that at 120 K (4%), and far too large for statistical deposition into the second layer. The height analysis thus confirms that the upward layer mass transport is possible during growth at 150 K also for an island at the step edge.

At a percentage of 26%, it is surprising that no islands exhibit atoms in the third layer as some atoms should have been accidentally deposited into this higher layer. Our results suggest that at the deposition temperature of 150 K, Co atoms deposited in the third layer are mobile enough to diffuse and descend to the bilayer and the upward mass transport is not significant. The absence of atoms in the third layer is consistent with the Co layer closing at 2.2 ML coverage in room-temperature growth corresponding to a layer-by-layer growth mode [18], i.e., a double layer. *Ab initio* studies for a related system, Co on Cu(001), related the stability of the bilayer film to the preference of the Co atoms to high coordination of alike atoms accompanied by a substantial contraction of the interlayer distance between the cobalt layers [44]. This energy contribution stabilizes the bilayers.

Concerning the lateral size, the island area varies from 1 to 42 nm^2 [Fig. 8(d)] with a median value of 13.9 nm^2. In contrast to the growth at 120 K [Fig. 4(d)], the area distribution is bimodal. Separating islands of different heights reveals that the first maximum in the bimodal distribution is caused by islands of bilayer height [Fig. 8(d)]. Their mean area, at (3.4 ± 1.9) nm^2, is considerably smaller than the one for the monatomic layer high island, at (18.2 ± 9.4) nm^2.

Also for the islands grown on terraces at 150 K [Fig. 9(a)], the number of islands with atoms in the second layer, at a height of (0.38 ± 0.02) nm, is, at approximately 19% [Figs. 9(b) and 9(c)], considerably larger than that of 5% at 120 K. This larger amount of bilayer high islands further confirms the upward mass transport for islands on terraces at 150 K.

On the other hand, the size distribution of Co islands grown on the terrace at 150 K is not bimodal. The area extends almost double the size range from ≈1 to ≈90 nm^2 with a median value of 12.8 nm^2 [Fig. 9(d)]. The area distribution of bilayer high islands spreads around the same range as the monolayer high islands. The mean area of (18.8 ± 17.2) nm^2 for the monolayer islands on terraces is consistent with the mean value of (18.2 ± 9.4) nm^2 for the islands of the same height at the step edges. However, the mean area of bilayer islands at (37.1 ± 21.7) nm^2 on terraces is significantly larger than that at (3.4 ± 1.9) nm^2 at step edges.

The most striking difference between islands grown on terraces as compared to those grown at step edges is their shape [cf. Fig. 8(a) to Fig. 9(a)]. The Co islands on terraces exhibit longer and more branched arms; the island shape is ramified [35]. We tentatively explain the difference in the island size distribution to the ramified growth process.

D. Growth of Co on Cu(111) at room temperature

In previous sections, we showed that the upward mass transport already leads to a measurable increase in the height of Co islands at a temperature of 150 K. It suggests that the amount of bilayer high islands increases with temperature.

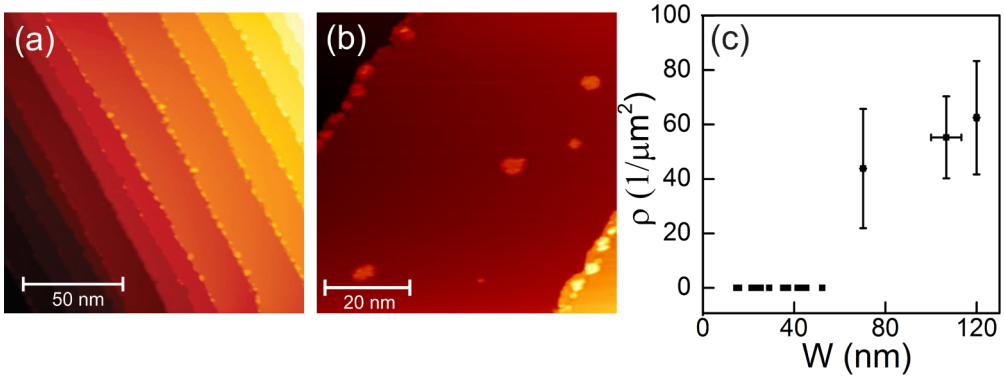

FIG. 10. Growth of Co island at room temperature: (a) region of surface with small terraces with $\langle d \rangle = (14.8 \pm 4.9)$ nm (860 mV, 0.5 nA, RT); (b) region of surface with a wide terrace of $W = (65 \pm 1)$ nm (860 mV, 0.6 nA, 0.04 ML, RT); and (c) dependence of island density ρ on terrace width W.

Previous studies investigated the Co growth only at coverages larger than 0.1 ML and at room temperature [24,25] and discussed only bilayer high islands nucleated on terraces. These islands are triangular in shape, and very different from the shape that we observed at lower temperature and coverage. We thus investigate the growth of Co at room temperature at a lower coverage of around 0.04 ML, in order to compare with our study at lower temperature. Indeed, a different type of island is found.

At room temperature, Co islands exclusively decorate step edges for small terraces with a mean width of (19.9 ± 4.2) nm [Fig. 10(a)], but nucleate homogeneously on rather broad terraces, e.g., with a width of (65 ± 1) nm [Fig. 10(b)]. The transition here is between 52 nm and 70 nm [Fig. 10(c)], reflecting a larger diffusivity at the higher deposition temperature.

The nucleation of islands at upper step edges, as at 120 and 150 K [Figs. 11(a) and 11(b)], indicates that at room temperature alloying at the step edge reduces the mobility of the adatoms close to it. Note that there are more islands of larger height on the right than on the left step edge. The reason is a varying local coverage at step edges that depends on the width of the upper terrace for smaller terraces.

The amount of islands with atoms in the second layer, at a height of (0.40 ± 0.02) nm, is at a percentage of 32%, which is only slightly higher than that at the lower growth temperature of 150 K [Figs. 11(b) and 11(c)]. There are two reasons for this result. First, the Co island edges at step edges are straighter than those at lower temperatures with considerably less kink sites (Fig. 1). Therefore, the calculated larger energy barrier for the upward mass transport of 0.66 eV at a B step and 0.91 eV at an A step [12] limits the upward mass transport, not the lower energy barrier of (0.19 ± 0.04) eV determined above for the upward mass transport at kink sites. Second, the increased alloying close to the step edge reduces the diffusion barrier close to the islands and thus the material available for growth. This is corroborated by the area distribution.

The island area varies similarly from 1 to 41 nm^2 as the one at 150 K growth with a median value of 5.5 nm^2 [Fig. 11(d)]. For the two types of islands of different heights, the mean island areas differ considerably, at (5.4 ± 4.2) nm^2 and (18.8 ± 8.3) nm^2 for monatomic layer islands and bilayer high islands, respectively. The mean area of bilayer high islands is, at room temperature, significantly larger than the one of (3.4 ± 1.9) nm^2 at 150 K. Only on islands larger than 10 nm^2 could the second layer be stable.

We conclude that at step edges, only slightly more islands are of bilayer height at room temperature than at 150 K. Our result is in contrast to previous studies [24,25], which found exclusively bilayer high islands at room temperature. As these studies analyzed only islands on terraces, we now characterize the island height and area on terraces at room temperature.

Surprisingly, there are two types of islands that differ in shape and size, as shown in Figs. 12(a) and 12(b). One type is rather compact and hexagonal in shape [Fig. 12(a)], while the other one is more irregular and triangular in shape [Fig. 12(b)]. Note the bright rim around the island in Fig. 12(b). Compact Co islands but with triangular shape were observed

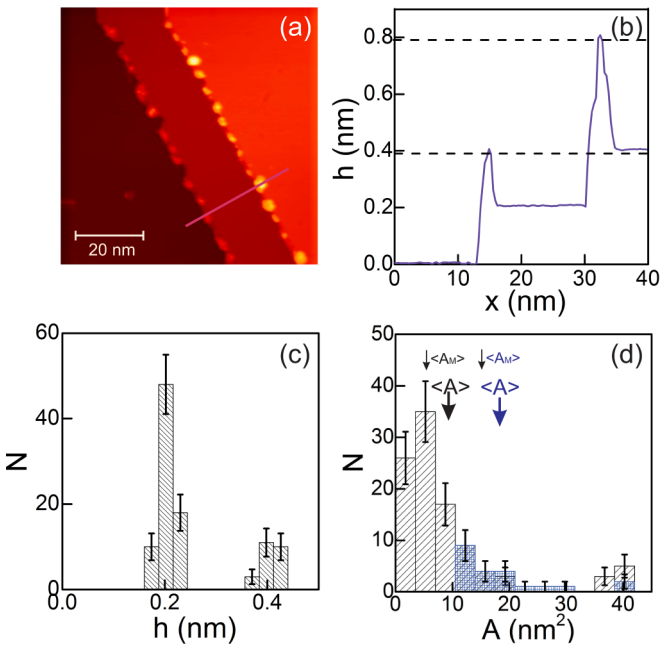

FIG. 11. Co island growth on step edges at room temperature: (a) STM image (860 mV, 0.6 nA, 0.04 ML, RT); (b) Line profile across the step edge along the line as shown in (a). Dashed lines mark the measured height of Co islands. (c) Height distribution. (d) Area distribution of all islands in gray. Bilayer islands in blue. A_M is the median value. $\langle A \rangle$ is the mean value.

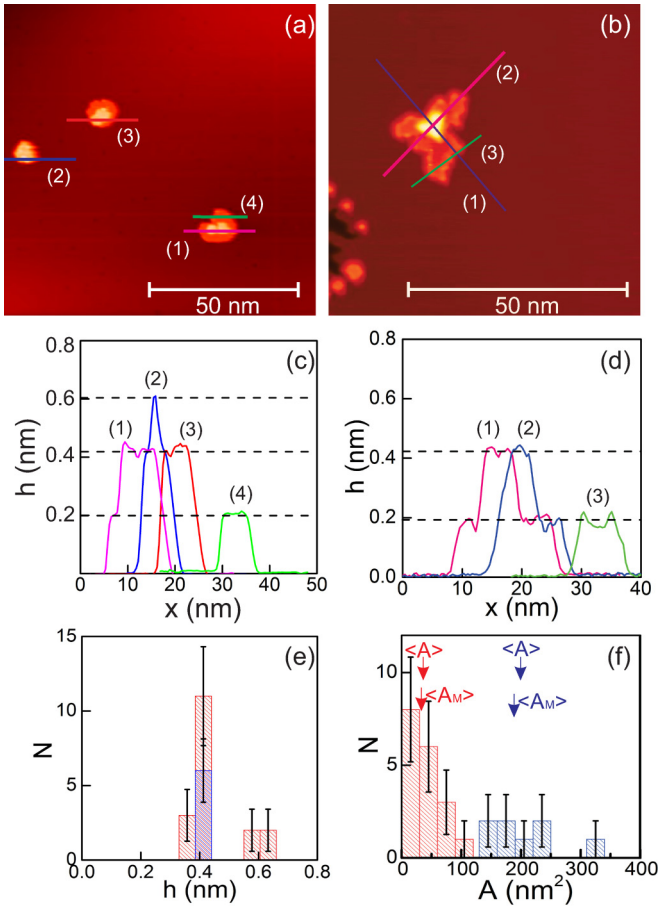

FIG. 12. Growth of Co islands on terraces at room temperature: (a) STM image of islands with compact hexagonal shape (860 mV, 0.5 nA, 0.04 ML, RT); (b) STM image of island with irregular triangular shape (−860 mV, 0.6 nA, 0.03 ML, RT); (c),(d) Line profiles along the lines shown in (a) and (b). The dashed lines are measured heights of Co islands. (e) Height distribution for both type of islands: compact hexagonal islands in red, irregular triangular islands in blue. (f) Area distribution. A_M is median value. $\langle A \rangle$ is mean value.

in other studies of epitaxial growth of Co/Cu(111) at room temperature [24,25]. A compact hexagonal shape is possible if energy barriers for crossing island corners can be overcome in both directions with equal probability, while a triangular shape points to an asymmetry in this barrier [41,42]. These barriers for corner crossing were determined to be 0.58 eV from A steps to B steps and 0.64 eV from B steps to A steps [12], values that are indeed important at room temperature. However, it is surprising that at the same growth temperature, the barrier can be surmounted in both directions for our islands, but not in previous works [24,25]. As the kinetics depends not only on temperature, but also on deposition rate, the different shape can be explained by the different deposition rate of $(3.5 \pm 0.5) \times 10^{-2}$ ML/min in our case and of ≈2.4 ML/min in Ref. [25]. The two orders of magnitudes lower deposition rate gives the islands enough time for equilibration to the thermodynamically preferred hexagonal shape and we conclude that triangular islands at the higher growth rate are kinetically limited structures.

The two types of islands do not only differ in shape, but also in height and size [Figs. 12(c) to 12(e)]. Irregular triangular islands are exclusively of bilayer height, at (0.40 ± 0.01) nm [Fig. 12(e)], and their areas range from ≈135 to ≈326 nm^2 with a median at 189.3 nm^2 and a mean value at (203.2 ± 62.1) nm^2 [Fig. 12(f)]. For compact hexagonal islands, a maximum in the height distribution at (0.61 ± 0.01) nm reveals growth in the third layer [Fig. 12(e)], but the heights are all smaller than ≈120 nm^2 with a median value of 32.4 nm^2 and a mean at (37.5 ± 26.9) nm^2.

A striking difference between the two island types is deduced from line profiles across the monolayer region [cf. line no. 4 in Fig. 12(c) to line no. 3 in Fig. 12(d)]. The island surface is smooth for the compact hexagonally shaped islands [Fig. 12(c)], while it is rough for the triangular-shaped island [Fig. 12(d)]. The border around the triangular-shaped islands is higher than its inner part. The rough surface of the triangular-shaped structures indicates that they are an alloy [45], while the smooth surface of the hexagonal-shaped islands indicates that they consist of one element only.

We refer to a study by Gomez *et al.* [23] based on Monte Carlo simulations in order to explain why islands of two different shapes form on terraces and what the mechanism is for the growth of irregular-shaped islands. The simulations found that an epitaxial triangular Co island of monolayer height lifts Cu atoms from the surface below, leading to the growth of an intermixed Co/Cu island and the appearance of a vacancy island. At room temperature, the distinct sizes of these two shapes observed here suggest that alloying is only feasible above an island size of approximate 135 nm^2. This explanation is in line with the fact that the island's surface is mainly rough at its border and less so in its interior. This border alloy causes the irregular shape of the islands as it influences the step diffusion barrier similar to the effect of the step edge alloy on the terrace diffusion discussed above [23], thus reducing the mobility along the step edge. In the following, we relate the alloying to the hexagonal depressions found after room-temperature growth [Figs. 1(h)].

Depressions are created mostly, but not exclusively, close to step edges [Fig. 13(a)]. With a depth of (0.21 ± 0.01) nm [Figs. 13(b) and 13(c)], they are identified as monolayer deep vacancy islands. Their appearance is related to the etching of Co into Cu discussed above [23]. The thus created small clusters of vacancies are mobile at room temperature [46]. They thus agglomerate to larger vacancy islands of the observed hexagonal equilibrium shape [43,47]. The area histogram of the vacancy islands reflects this Smoluchowski ripening [48,49] with a wide range of areas from 1 to 250 nm^2, but with the majority of the vacancy islands having areas of less than 50 nm^2 [Fig. 13(d)]. The appearance of vacancy islands on terraces supports the idea that intermixed islands are formed at room temperature. Reversely, the absence of vacancy islands at the lower investigated temperatures supports our earlier conclusion that the islands are pure Co islands.

IV. DISCUSSION

Though we have already pointed out similarities and differences between islands grown at the three investigated temperatures in the sections above, we now compare their

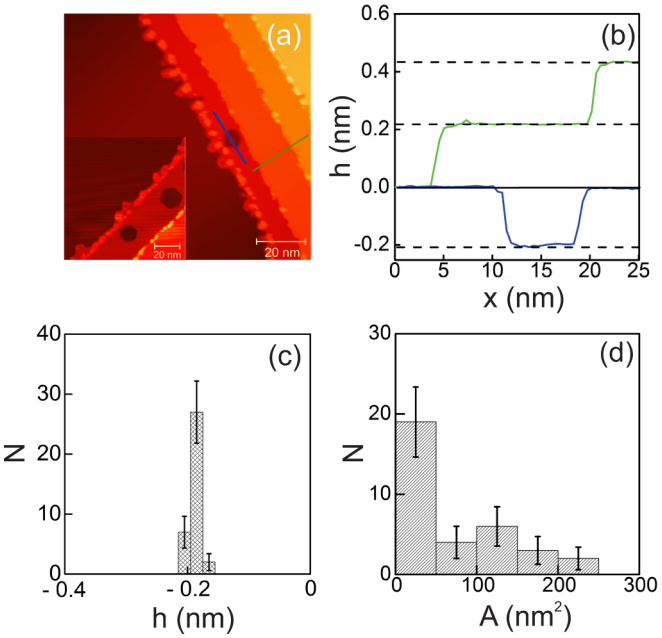

FIG. 13. Growth of Co vacancy islands at step edges at room temperature: (a) STM image of region with small terraces with a vacancy island next to a step edge (−860 mV, 0.8 nA, 0.03 ML, RT); inset: region of surface with two hexagonal vacancy islands on a terrace (856 mV, 0.6 nA, 0.03 ML, RT). (b) Line profiles along the lines as shown in (a). The dashed lines indicate measured heights of an atomic layer of Cu(111). (c) Vacancy island depth distribution. (d) Vacancy island area distribution.

density, height, and area directly for a final discussion. Concerning the heights (Table I), the increase of bilayer high islands from 120 to 150 K is comparable both at step edges and on terraces. However, there is a large increase of this island type between 150 and 300 K on terraces, while there is only a moderate one at step edges. In addition, trilayer high islands have a significant amount only on terraces at 300 K, while no pure monatomic high islands are observed. The absence of only monatomic layer high islands on terraces at 300 K indicates that Co atoms diffuse to the second layer more easily on the terrace grown islands than on the step edge grown ones. As described above, the influence of additional diffusion barriers of 0.10 and 0.24 eV close to the step edges due to alloying [23] also leads to the increased binding energy of Co atoms on the Cu substrate, and thus to less upward mass transport. The prerequisite for forming a third layer, i.e., the existence of bilayer high islands, is thus much more abundant on terraces than at step edges.

TABLE I. Ratio of 1, 2, and 3 ML high islands at step edges and on terraces.

	At step edges		On terraces		
Height	1 ML	2 ML	1 ML	2 ML	3 ML
120 K	96%	4%	95%	5%	0%
150 K	74%	26%	81%	19%	0%
300 K	68%	32%	0%	78%	22%

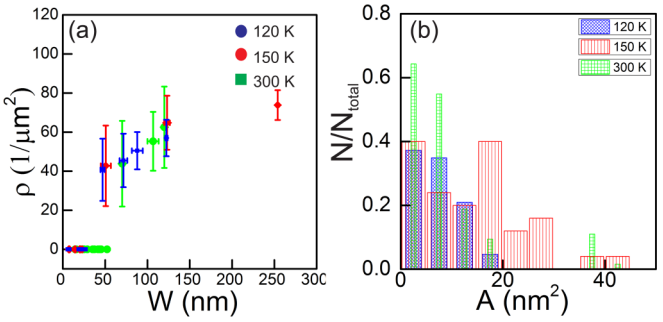

FIG. 14. Comparison of island density and area for three growth temperatures: (a) Dependence of Co islands density ρ on the terrace width W. (b) Normalized area histograms at step edges.

The dependence of the Co island density ρ on terrace width W shows that for homogeneous nucleation, larger terrace widths are needed at high temperature due to the increased mobility of the atoms [Fig. 14(a)]. However, the increase is smaller than expected, which implies that the nucleation density does not differ by a large factor. This surprising observation suggests that the diffusion barrier is reduced at higher temperature. We propose that the alloying-induced embedded Co adatoms in the surface lead to the reduction of the surface diffusion barrier of Co on Cu(111). Such a decreased diffusion energy caused by embedded atoms was observed previously both in the experiment on Pb/Cu(111) [50] and in the theoretical calculations on Cu/Sn(111) alloy surfaces [51].

Finally, we compare the normalized area of islands at step edges [Fig. 14 and Table II]. In contrast to islands on terraces, their shape does not largely change and thus tip convolution effects are not significant. We refrain from comparing the areas of the islands on terraces directly, as their shape changes significantly for different temperatures.

At step edges, the area of the islands at 150 and 300 K varies in a wider range than at 120 K. The area ranges at 150 and 300 K are approximately twice as broad as that at 120 K. In addition, the N vs A distribution is less monotonous. As explained above, such a nonmonotonous distribution indicates mobility-induced Smoluchowski ripening. The higher nucleation density at step edges facilitates this type of ripening. Thus, the additional energy barrier close to step edges leads to this different behavior. This behavior is supported by comparing the mean island areas at step edges (Table II). For the monatomic high islands, the mean island area at 150 K is larger by a factor of around 2 than the one at 120 K, but it decreases by a factor of 7 at 300 K as compared to the one at 150 K. For the bilayer high islands, the mean areas increase

TABLE II. Mean areas of 1 and 2 ML high islands at step edges.

	Area (nm²)	
	1 ML	2 ML
120 K	7.2 ± 3.9	
150 K	18.2 ± 9.4	3.4 ± 1.9
300 K	5.4 ± 4.2	18.8 ± 8.3

by a factor of 5 from 150 to 300 K. While the increase in mean island size of bilayer high islands just reflects the larger mobility of Co adatoms at higher temperature, the decrease of the mean island size of monolayer high islands implies that larger islands facilitate the upward mass transport transforming monolayer high islands into bilayer high islands.

V. CONCLUSION

We presented an extensive data set for the growth of Co on Cu (111) at a coverage between 0.03 and 0.04 ML from 120 to 300 K for understanding the growth of this important material combination in a wide range of temperatures. We determined a rather low activation energy for the upward layer mass transport of $E_{\text{upward}} = (0.15 \pm 0.04)$ eV at low temperature. We explain this low value by the kinked nature of step edges at low temperature, which leads to a different value than the calculated one [12]. Furthermore, we showed that surface alloy formation is an important factor to be considered in nucleation at step edges already at cryogenic temperature. A major influence of alloying is found at room-temperature growth, in particular for larger islands on the terrace. This alloying will influence the magnetic properties of the nanostructures.

The used approaches can be applied to investigations of the growth of Co on other metal substrates. On a more general footing, alloying is an important issue to be considered in transition-metal growth, as suggested recently for the case of Cu/Ag(100) [45,52,53].

[1] T. Michely and J. Krug, *Islands, Mounds, and Atoms*, (Springer, New York, 2004).
[2] M. C. Tringides, *Surface Diffusion: Atomistic and Collective Processes*, NATO ASI Series B: Physics (Plenum, New York, 1997), Vol. 360.
[3] Y. Ohno, D. K. Young, B. Beschoten, F. Matsukura, H. Ohno, and D. D. Awschalom, Nature (London) **402**, 790 (1999).
[4] C. Chappert, A. Fert, and F. N. V. Dau, Nat. Mater. **6**, 813 (2007).
[5] N. Mott, Adv. Phys. **13**, 325 (1964).
[6] A. Fert and I. A. Campbell, Phys. Rev. Lett. **21**, 1190 (1968).
[7] A. Fert and I. A. Campbell, J. Phys. F **6**, 849 (1976).
[8] M. Ohring, *Materials Science of Thin Films*, (Academic, New York, 2002).
[9] K. Tanaka, Materials **3**, 4518 (2010).
[10] J. J. de Miguel and R. Miranda, J. Phys.: Condens. Matter **14**, R1063 (2002).
[11] K. Morgenstern, J. Kibsgaard, J. V. Lauritsen, E. Laegsgaard, and F. Besenbacher, Surf. Sci. **601**, 1967 (2007).
[12] N. N. Negulyaev, V. S. Stepanyuk, P. Bruno, L. Diekhöner, P. Wahl, and K. Kern, Phys. Rev. B **77**, 125437 (2008).
[13] N. Zaki, D. Potapenko, P. D. Johnson, and R. M. Osgood, Phys. Rev. B **80**, 155419 (2009).
[14] D. Turko, I. Morawski, and M. Nowicki, Vacuum **85**, 768 (2011).
[15] G. J. Mankey, R. F. Willis, and F. J. Himpsel, Phys. Rev. B **47**, 190 (1993).
[16] L. Diekhöner, M. A. Schneider, A. N. Baranov, V. S. Stepanyuk, P. Bruno, and K. Kern, Phys. Rev. Lett. **90**, 236801 (2003).
[17] P. Huang and E. A. Carter, Nano Lett. **6**, 1146 (2006).
[18] J. Bork, L. Diekhöner, Z. Li, and J. Onsgaard, Surf. Sci. **604**, 1536 (2010).
[19] D. Böttcher, A. Ernst, and J. Henk, J. Phys.: Condens. Matter **23**, 296003 (2011).
[20] S.-C. Wang, M. B. Yilmaz, K. R. Knox, N. Zaki, J. I. Dadap, T. Valla, P. D. Johnson, and R. M. Osgood, Jr, Phys. Rev. B **77**, 115448 (2008).
[21] E. Michel, H. Ibach, and C. M. Schneider, Phys. Rev. B **92**, 024407 (2015).
[22] B. W. Heinrich, C. Iacovia, M. V. Rastei, L. Limot, P. A. Ignatiev, V. S. Stepanyuk, and J. P. Bucher, Eur. Phys. J. B **75**, 49 (2010).
[23] L. Gómez, C. Slutzky, J. Ferron, J. de la Figuera, J. Camarero, A. L. Vázquez de Parga, J. J. de Miguel, and R. Miranda, Phys. Rev. Lett. **84**, 4397 (2000).
[24] J. de la Figuera, J. E. Prieto, C. Ocal, and R. Miranda, Phys. Rev. B **47**, 13043 (1993).
[25] J. E. Prieto, J. de la Figuera, and R. Miranda, Phys. Rev. B **62**, 2126 (2000).
[26] J. de la Figuera, J. E. Prieto, G. Kostka, S. Müller, C. Ocal, R. Miranda, and K. Heinz, Surf. Sci. **349**, L139 (1996).
[27] K. Heinz, S. Müller, and L. Hammer, J. Phys.: Condens. Matter **11**, 9437 (1999).
[28] I. Horcas, R. Fernandez, J. M. Gomez-Rodriguez, J. Colchero, J. Gomez-Herrero, and A. M. Baro, Rev. Sci. Instrum. **78**, 013705 (2007).
[29] T. Michely, M. Hohage, M. Bott, and G. Comsa, Phys. Rev. Lett. **70**, 3943 (1993).
[30] H. Röder, K. Bromann, H. Brune, and K. Kern, Phys. Rev. Lett. **74**, 3217 (1995).
[31] H. Brune, Surf. Sci. Rep. **31**, 125 (1998).
[32] E. Cox, M. Li, P.-W. Chung, C. Ghosh, T. S. Rahman, C. J. Jenks, J. W. Evans, and P. A. Thiel, Phys. Rev. B **71**, 115414 (2005).
[33] J. Shen, R. Skomski, M. Klaua, H. Jenniches, S. S. Manoharan, and J. Kirschner, Phys. Rev. B **56**, 2340 (1997).
[34] J. A. Venables, G. D. T. Spiller, and M. Hanbücken, Rep. Prog. Phys. **47**, 399 (1984).
[35] Q. H. Vu and K. Morgenstern (unpublished).
[36] K. Morgenstern, Phys. Status Solidi B **242**, 773 (2005).
[37] K. Morgenstern, G. Rosenfeld, and G. Comsa, Phys. Rev. Lett. **76**, 2113 (1996).
[38] K. Morgenstern, G. Rosenfeld, E. Lægsgaard, F. Besenbacher, and G. Comsa, Phys. Rev. Lett. **80**, 556 (1998).
[39] P. A. Thiel, M. Shen, D. J. Liu, and J. W. Evans, J. Phys. Chem. C **113**, 5047 (2009).
[40] Y. Han, S. M. Russell, A. R. Layson, H. Walen, C. D. Yuen, P. A. Thiel, and J. W. Evans, Phys. Rev. B **87**, 155420 (2013).
[41] M. Bott, T. Michely, and G. Comsa, Surf. Sci. **272**, 161 (1992).
[42] M. Bott, M. Hohage, M. Morgenstern, T. Michely, and G. Comsa, Phys. Rev. Lett. **76**, 1304 (1996).
[43] M. Giesen, Prog. Surf. Sci. **68**, 1 (2001).
[44] R. Pentcheva and M. Scheffler, Phys. Rev. B **61**, 2211 (2000).

[45] C. Zaum, M. Rieger, K. Reuter, and K. Morgenstern, Phys. Rev. Lett. **107**, 046101 (2011).
[46] D. C. Schlößer, K. Morgenstern, L. K. Verheij, G. Rosenfeld, F. Besenbacher, and G. Comsa, Surf. Sci. **465**, 19 (2000).
[47] J. W. Evans, P. A. Thiel, and M. C. Bartelt, Surf. Sci. Rep. **61**, 1 (2006).
[48] C. R. Stoldt, C. J. Jenks, P. A. Thiel, A. M. Cadilhe, and J. W. Evans, J. Chem. Phys. **111**, 5157 (1999).
[49] G. Rosenfeld, K. Morgenstern, M. Esser, and G. Cosma, Appl. Phys. A **69**, 489 (1999).
[50] M. L. Anderson, N. C. Bartelt, P. J. Feibelman, B. S. Swartzentruber, and G. L. Kellogg, Surf. Sci. **600**, 1901 (2006).
[51] Z. Chen, N. Kioussis, K.-N. Tu, N. Ghoniem, and J.-M. Yang, Phys. Rev. Lett. **105**, 015703 (2010).
[52] A. Beichert, C. Zaum, and K. Morgenstern, Phys. Rev. B **92**, 045422 (2015).
[53] C. Zaum and K. Morgenstern, Nano Lett. **16**, 3001 (2016).